CrossMark

Numerical optimization of coordinated reset stimulation for desynchronizing neuronal network dynamics

Shigeru Kubota[1] · Jonathan E. Rubin[2]

Abstract

Excessive synchronization in neural activity is a hallmark of Parkinson's disease (PD). A promising technique for treating PD is coordinated reset (CR) neuromodulation in which a neural population is desynchronized by the delivery of spatially-distributed current stimuli using multiple electrodes. In this study, we perform numerical optimization to find the energy-optimal current waveform for desynchronizing neuronal network with CR stimulation, by proposing and applying a new optimization method based on the direct search algorithm. In the proposed optimization method, the stimulating current is described as a Fourier series, and each Fourier coefficient as well as the stimulation period are directly optimized by evaluating the order parameter, which quantifies the synchrony level, from network simulation. This direct optimization scheme has an advantage that arbitrary changes in the dynamical properties of the network can be taken into account in the search process. By harnessing this advantage, we demonstrate the significant influence of externally applied oscillatory inputs and non-random network topology on the efficacy of CR modulation. Our results suggest that the effectiveness of brain stimulation for desynchronization may depend on various factors modulating the dynamics of the target network. We also discuss the possible relevance of the results to the efficacy of the stimulation in PD treatment.

Keywords Parkinson's disease · Brain stimulation · Coordinated reset · Synchronization · Numerical optimization

1 Introduction

Stimulation of local brain regions, such as the subthalamic nucleus (STN), with repeated current pulses is widely used for the treatment of Parkinson's disease (PD) (Kühn and Volkmann 2017; Herrington et al. 2016). Such brain stimulation has a well-established clinical effect of improving the major symptoms of PD (e.g., rigidity and tremor) as well as the quality of life (Benabid et al. 2009) in certain patient populations. On the other hand, despite the accumulation of

✉ Shigeru Kubota
  kubota@yz.yamagata-u.ac.jp

[1] Graduate School of Science and Engineering, Yamagata University, 4-3-16 Jonan, Yonezawa, Yamagata 992-8510, Japan

[2] Department of Mathematics, University of Pittsburgh, 301 Thackeray Hall, Pittsburgh, PA 15260, USA

knowledge on the related neurophysiology, the methodology of brain stimulation has not been substantively changed over the decades since its introduction (Wang et al. 2016; Brocker et al. 2017). One of the problems to be solved for this treatment is that the life span of implanted stimulators is much shorter than the life expectancy of many patients, meaning that multiple surgeries are necessary to replace the stimulating device over the treatment period (Foutz and McIntyre 2010). Prolonging stimulator battery life would require a stimulus delivery method that can directly target the pathological process and decrease the energy consumption (Foutz and McIntyre 2010; Wang et al. 2016). Further, stimulation with smaller current magnitudes is quite important for avoiding side effects (e.g., stimulation-induced dyskinesia), which could be created by the spread of current to the brain structures surrounding the electrode (Benabid et al. 2009). Similar considerations apply to thalamic stimulation, which has a long history of use for essential tremor and parkinsonian tremor (Ondo et al. 1998; Kumar et al. 2003; Baizabal-Carvallo et al. 2014). Motor cortex stimulation (MCS) also shows promise for improving parkinsonian motor symptoms (Drouot et al. 2004; Gaynor et al. 2008; Lavano et al.

2017), and the development of this technology should focus on energy-efficient approaches as well.

A promising technique to improve the efficiency of stimulation and reduce the energy consumption and potential adverse effects is coordinated reset (CR) neuromodulation (Tass 2003; Tass et al. 2012; Ebert et al. 2014; Wang et al. 2016). CR modulation involves the delivery of spatially-distributed pulse trains from multiple electrodes, which is hypothesized to separate a population of firing neurons into subgroups by resetting the phases of their activity. Accordingly, a synchronized network state, which is a hallmark of basal ganglia activity in parkinsonism (Rubin et al. 2012; Mallet et al. 2008; Gatev et al. 2006), may be switched into a desynchronized state. A key advantage of CR modulation is that its effects can be achieved with lower pulse amplitudes than are used in the conventional stimulation method (Wang et al. 2016). Recent experimental studies have shown that CR stimulation of STN can cause both acute and long-lasting improvement in the motor function of parkinsonian monkeys (Tass et al. 2012; Wang et al. 2016). Additionally, the effectiveness of the CR technique has been supported by a short-term trial in PD patients (Adamchic et al. 2014).

Energy-efficient current waveforms for brain stimulation have been investigated with various approaches, such as optimal control theory (Jezernik et al. 2010; Jezernik and Morari 2005; Forger et al. 2011), numerical optimization with genetic algorithms (Wongsarnpigoon and Grill 2010), and the detailed simulation (and experimental study) of neuronal activation (Sahin and Tie 2007; Foutz and McIntyre 2010; Wongsarnpigoon et al. 2010; see Grill 2015 for review). These studies have shown that the high-frequency pulsatile input, which is currently used for implantable stimulators, may not be energy efficient, and the optimization of waveform shapes may be required to minimize energy consumption. Further, recent studies (Wilson and Moehlis 2014a, 2014b) have also applied optimal control theory and revealed that a current waveform that leads to positive Lyapunov exponents in neuronal dynamics is more energy efficient than pulsatile stimuli for desynchronizing network activity. It can be expected from these studies that the energy consumption by CR neuromodulation could be further decreased by optimally selecting a stimulation waveform instead of using conventional pulse stimuli.

Therefore, in this study, we construct a model of a neuronal network with multiple stimulating currents and use it to numerically explore the energy-optimal current waveform for desynchronization of model neurons by CR neuromodulation. We propose an efficient optimization method in which the time course of stimuli is described by a second-order Fourier series, and each Fourier coefficient and the stimulation period are globally optimized through a direct search algorithm (Hooke and Jeeves 1961; Dixon 1972; Khambampati et al. 2010; Kubota et al. 2015) to achieve desynchronization. We show that the energy consumption is substantially lower when the Fourier input rather than the conventional pulse input is used for CR

modulation. In addition, we show that the effectiveness of the CR stimulation could be significantly modulated by the characteristics of network, such as the existence of external oscillatory inputs and non-random topological structure. These results serve to provide valuable insights relevant to the derivation of more effective and efficient stimulation techniques.

2 Methods

2.1 Network model

We constructed a model network consisting of $N = 100$ leaky integrate-and-fire (LIF) neurons. The neurons are spatially arranged on a grid within a square having a side length of 2 and a center at the origin (Fig. 1a). The membrane potential V_i of the ith neuron obeys the following equation:

$$\tau_m \frac{dV_i}{dt} = -(V_i - E_L) + RI_i, \qquad (1)$$

where $\tau_m = 20$ ms is the membrane time constant, $E_L = -74$ mV is the leak potential, $R = 40$ MΩ is the input resistance, and I_i is the input current (Troyer and Miller 1997; Liu and Wang 2001). The LIF neuron fires an action potential when the membrane potential rises to -54 mV. Subsequently, the membrane potential is reset to -74 mV and is kept at this value during an absolute refractory period of 2 ms.

All synapses between neurons are assumed to be excitatory. The synaptic current that the ith neuron receives is $I_{syn}^i = g_A s_A^i V_i$, corresponding to a reversal potential of 0 mV, with the peak conductance $g_A = 0.5$ nS. The activation variable s_A^i increases by 1 when a presynaptic cell fires and then it decays with a time constant of 5 ms (Izhikevich et al. 2004). The total input current to the ith neuron is described as

$$I_i = -I_{syn}^i + I_{stim,i}^{sum} + \eta_i + a_{com}\eta_{com}. \qquad (2)$$

Here, $I_{stim,i}^{sum}$ is the sum of the stimulating currents from all electrodes that are received by the ith neuron (see below). η_i denotes white Gaussian noise with mean μ_{ind} and standard deviation $0.1\mu_{ind}$, which is applied independently to each neuron at every integration time step of 0.5 ms. η_{com} represents white Gaussian noise that is applied to all model neurons and has mean μ_{com} and standard deviation $0.1\mu_{com}$. The intensity of this common input changes periodically with time according to the following equation:

$$a_{com} = \left(A_{com}^{max} - A_{com}^{min}\right)[\sin(2\pi f_{com}t) + 1]/2 + A_{com}^{min}, \qquad (3)$$

where $A_{com}^{max} = 1$, $A_{com}^{min} = 0.1$, and $f_{com} = 25$ Hz. In all figures except for Fig. 5, only the independent noise is applied, without the common noise, by setting $\mu_{ind} = 0.52$ nA and $\mu_{com} = 0$ nA. In Fig. 5, the common noise is introduced by setting
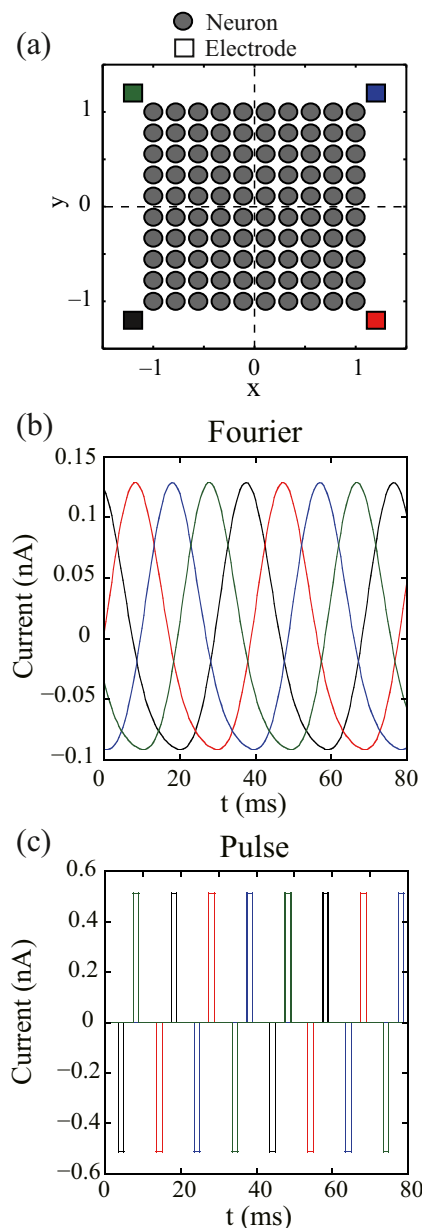
Fig. 1 Set-up of network and stimulation. **a** In the network model, 100 LIF neurons are arranged on a planar grid such that their positions in the x-y plane are $\{(n_x\Delta x - 1, n_y\Delta y - 1)|n_x, n_y = 0, 1, \cdots, 9\}(\Delta x = \Delta y = 2/9)$. The four stimulation electrodes are placed at the corners of the grid with coordinates $(\pm 1, \pm 1)$. (**b** and **c**) Examples of the optimal current waveforms for Fourier inputs (**b**) and symmetric pulse inputs (**c**). The weight parameter $\alpha = 3.1$ nA^{-2}·mS is used for the optimization in this example. Each current shown in (**b**) and (**c**) is delivered by the electrode represented with the same color in (**a**)

μ_{com} to a positive value. In this case, to maintain the overall level of the sum of the two types of noise, μ_{ind} is altered as function of μ_{com} by maintaining the relation of $\mu_{ind} + \mu_{com} \left(A_{com}^{max} + A_{com}^{min}\right)/2 = 0.52$ (in nA).

In the simulations except those for Fig. 6, we used a random network where a synaptic connection from any one neuron to another is randomly introduced with the probability of 0.2. In Fig. 6, we made a comparison between networks with

random and small-world topologies (Watts and Strogatz 1998). Here, we first generated a planar regular network, in which each neuron has bidirectional connections with the neurons surrounding it, and then each connection was randomly rewired, similar to the algorithm presented in Prettejohn et al. (2011). The rewiring probability was set to 1 and 0.06 for the random and small-world networks, respectively. The random rewiring of a regular network leads to an increase in the number of the neuron pairs with unidirectional connections (n_1) and a decrease in the number of the neuron pairs with bidirectional connections (n_2). Accordingly, the random network has larger n_1 and smaller n_2 values than the small world, while the total number of connections (i.e., $n_1 + 2n_2$) is the same for the two networks. In the networks used in Fig. 6, $(n_1,n_2) = (670, 7)$ and (40, 322) for the random and small-world connectivity, respectively, with $n_1 + 2n_2 = 684$ for both cases. To elucidate the effect of changing the network topology without changing the values of n_1 and n_2, we additionally consider a network with a connectivity that is randomly selected under the condition that both the n_1 and n_2 values are the same as those of the small world (i.e., $(n_1,n_2) = (40, 322)$) in Fig. 6e (blue line).

2.2 Current stimulation

To simulate the CR modulation, we introduced $M = 4$ electrodes located at the corners of the network (Tass 2003) (Fig. 1a). The waveform of stimulating currents (Fig. 1b) is described with a Fourier series as follows:

$$I_{stim}^j = I_0 f_{stim}\left(t - \frac{(j-1)T}{M}\right), \tag{4}$$

$$f_{stim}(t) = \sum_{n=1}^{p}\left(a_n\cos\frac{2n\pi t}{T} + b_n\sin\frac{2\pi n t}{T}\right). \tag{5}$$

Here, I_{stim}^j $(j = 1,\cdots,M)$ is the current generated by the jth electrode, $I_0 = 0.4$ nA is a parameter to set the current magnitude, T is the stimulation period, and a_n and b_n $(n = 1,\cdots,p)$ are the Fourier coefficients. As shown in Eq. (4), the phases of currents produced by the M electrodes are equally spaced in $[0, 2\pi]$. We assumed $p = 2$ throughout this study, since the results of optimization were not improved with a larger value of p. Note that the constant term in the Fourier series is removed to make the integral of the current equal to zero, because charge balance is important to prevent damage of the electrode and of neuronal tissue due to charge transfer (Ebert et al. 2014; Cogan 2008; Cogan et al. 2006).

The total current stimulation received by the ith neuron is described as

$$I_{stim,i}^{sum} = \sum_{j=1}^{M} \sigma_{ij} I_{stim}^j. \tag{6}$$

Here, σ_{ij} represents the impact of the stimulus from the jth electrode on the ith neuron, which decays with the unitless

relative distance measure d_{ij} between the electrode and neuron as follows:

$$\sigma_{ij} = \min\left(\frac{1}{d_{ij}l_c\sqrt{1 + 4(d_{ij}/l_c)^2}}, \sigma_c\right), \qquad (7)$$

with $\sigma_c = 1$ (i.e., with σ_{ij} normalized to be less than or equal to 1) and $l_c = 2$ (Ebert et al. 2014).

For comparison to the Fourier inputs, we also tested conventional pulse-train inputs (Fig. 1c). To model the application of pulse inputs, $f_{stim}(t)$ in Eq. (5) is replaced by the following equations:

$$f_{stim}(t) = A_p G\left(t - t_p\right) - A_p G\left(t - t_p - y_p\right), \qquad (8)$$

$$G(t) = H(\sin(2\pi t/T)) \times \left[1 - H\left(\sin\left(2\pi\left(t - \delta_p\right)/T\right)\right)\right], \qquad (9)$$

where $H(x)$ is the Heaviside step function satisfying $H(x) = 1$ for $x \geq 0$ and $H(x) = 0$ for $x < 0$. The pulse inputs are biphasic and symmetric, i.e., composed of brief depolarizing and hyperpolarizing pulses with the same magnitude, to maintain charge balance as in the case of Fourier inputs (Ebert et al. 2014). A_p and δ_p are the amplitude and width of the symmetric pulses, respectively. The pulse width is assumed to be within a range of $\delta_p \leq 1.5$ ms, which includes typical values used for PD treatment (Kuncel and Grill 2004; Reich et al. 2015; Brocker et al. 2017). y_p is the time lag between the depolarizing and hyperpolarizing pulses, and t_p sets the timing for eliciting the depolarizing pulse.

In one figure (Fig. S1, supplementary material), we additionally examined the biphasic asymmetric pulse, in which the hyperpolarizing pulse has longer temporal width and smaller amplitude than the depolarizing pulse (Fig. S1a) (Cogan 2008; Cogan et al. 2006; Fan et al. 2016; Hofmann et al. 2011). The asymmetric pulse is frequently used for deep brain stimulation (DBS) to minimize the polarization by the charge-balancing pulse (Cogan 2008; Cogan et al. 2006). In cases where the asymmetric pulse is applied, $f_{stim}(t)$ in Eq. 5 is replaced by the following equations (Fan et al. 2016):

$$f_{stim}(t) = A_r F(G(t - t_r)), \qquad (10)$$

$$F(x) = \begin{cases} 1, & (x = 1), \\ -\delta_p / (T - \delta_p), & (x = 0), \end{cases} \qquad (11)$$

Here, A_r and δ_p are the amplitude and width of the depolarizing pulse, respectively, and t_r determines the pulse timing. The amplitude and width of the hyperpolarizing pulse are $A_r\delta_p/(T - \delta_p)$ and $T - \delta_p$, respectively, so that the charge balance is maintained.

2.3 Optimization search

We performed optimization of the current waveform for the CR stimuli to elucidate the stimulation method that can desynchronize the network with minimal energy consumption. For this purpose, the objective function to be minimized was defined as

$$J = \rho + \alpha E, \qquad (12)$$

where ρ is the average order parameter to signify the level of synchrony (see below), E is the rate of the energy consumption per unit time, and α is a positive weighting parameter. The energy consumption rate is described by the following equation:

$$E = \sum_{j=1}^{M} (1/T)\int_0^T \left\{I_{stim}^j(t)\right\}^2 Z(t)dt, \qquad (13)$$

where the impedance $Z(t)$ is simply assumed to be constant ($Z(t) = 1$ kΩ) (Foutz and McIntyre 2010). From network simulation during current stimulation, we obtained the time course of order parameter $r(t)$ as follows:

$$r(t) = \left|\frac{1}{N}\sum_{j=1}^{N} e^{i\phi_j(t)}\right|. \qquad (14)$$

Here, ϕ_j is the firing phase of the jth neuron, defined as $\phi_j(t) = 2\pi(t - t_{j,k})/(t_{j,k+1} - t_{j,k})$ for $t_{j,k} \leq t < t_{j,k+1}$, where $t_{j,k}$ is the kth firing time of the jth neuron (Ebert et al. 2014). To estimate the average order parameter ρ, the network simulation was performed 32 times using different random number sequences, and the trial and temporal average of $r(t)$ was taken as follows:

$$\rho = \left\langle (1/T_a)\int_{t_0}^{t_0+T_a} r(t)dt \right\rangle, \qquad (15)$$

where the angular brackets denote a trial average and $T_a = 5$ s is the interval for temporal averaging.

To optimize the Fourier inputs, we performed an optimization search to find the values of a_n and b_n ($n = 1, \cdots, p$) and T (Eqs. (4) and (5)) that minimize the value of objective function J. Similarly, we conducted optimization over the values of A_p, t_p, y_p, δ_p, and T (Eqs. (8) and (9)) for the symmetric pulses, and over the values of A_r, t_r, δ_p, and T (Eqs. (10) and (11)) for the asymmetric pulses, to minimize the J value.

For the optimization algorithm, we used the pattern search, which is a widely used direct search method (Hooke and Jeeves 1961; Dixon 1972; Khambampati et al. 2010; Kubota et al. 2015). In this algorithm, the two phases called exploratory moves and pattern moves are iterated alternately. In an exploratory move, the search point locally moves around in all directions in the parameter space near the base point $\mathbf{x_b}$, which is the starting search point of the exploratory move. Let us define $\mathbf{x_n}$ and $\mathbf{x_p}$ as the points that provide the best objective function value among the points visited in the exploratory move for the current and previous iteration, respectively. Then, in the pattern move, the base point makes a relatively long move such that $\mathbf{x_b} \leftarrow \mathbf{x_n} + (\mathbf{x_n} - \mathbf{x_p})$, where $\mathbf{x_n} - \mathbf{x_p}$ is a

vector that represents the best search direction predicted at the present time. The new base point becomes the starting point of the exploratory move for the next step. The use of the pattern move is important to accelerate the search speed by using the information regarding the objective function obtained in the past. The pattern search is finished in cases where the base point reaches a local optimal solution at which the objective function value cannot be improved by the exploratory move. To perform global search in the parameter space, we repeated the pattern search 8 times from randomly selected starting points and adopted the solution providing the smallest J value as an estimate of the global optimal solution.

When the weight parameter α is sufficiently large, the magnitude of the stimulating current converges to zero (i.e., $E = 0$) at the optimal solution. This implies that the optimal stimulus is too weak to be detected by the current optimization search. Therefore, an upper bound on the weight parameter is imposed.

2.4 Numerical simulation

The network model was implemented in the C++ language. The optimization search was executed by repetitively running the executable file, generated by compiling the C++ source code, from a MATLAB program. Finding a global optimal solution for each case requires 1000 iterations of objective function evaluation, which correspond to 16 h on an Intel Xeon E5–2660 v4 personal computer (2.00 GHz). The source codes are available upon request.

3 Results

3.1 Optimization of the current waveform for CR modulation

To explore an energy efficient method for brain stimulation, we constructed a network model (Fig. 1a) and performed optimization of the current waveform for CR modulation to decrease the energy consumption for desynchronization. The curves in Fig. 1b show the time courses of the optimized stimuli given by the four electrodes in Fig. 1a. Here, we applied an optimization method in which the current waveform is described as a second-order Fourier series, and each Fourier coefficient and the stimulation period are optimized to minimize the value of an objective function (Eq. (12)). Since the oscillatory phases of the Fourier inputs from the four electrodes are different, the population of firing neurons may become divided into subgroups (Tass 2003). Consistent with this idea, we find that application of the optimal Fourier stimuli can rapidly decrease the order parameter, producing a desynchronized state, as shown in Fig. 2 (solid line). In fact, the dynamics of the stimulated neuronal population depends
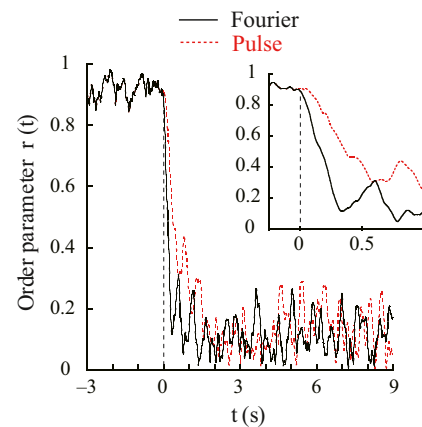

Fig. 2 The time course of order parameter $r(t)$. The order parameter decreases following the onset of the optimal stimulation (at $t = 0$) with the Fourier (black) and symmetric pulse (red) inputs. The weight parameter $\alpha = 3.1$ nA^{-2}·mS is used for the optimization. The inset shows the magnification of the two curves around $t = 0$. The network state without stimulation (i.e., $t < 0$) is characterized by an average order parameter of $\rho = 0.914$ and a firing rate of 21.3 Hz

on the value of the objective function weight parameter α (Eq. (12)), as we shall discuss below.

We also performed optimization of conventional symmetrically biphasic pulses (Eqs. (8) and (9); Fig. 1c), and examined the decrease in order parameter induced by the optimal pulse stimuli (Fig. 2, dashed line). The energy consumption required for the optimal pulse input ($E = 0.0786$ nA^2·kΩ) is 3 times larger than that for the optimal Fourier input ($E = 0.0246$ nA^2·kΩ), although the final levels of the order parameter achieved by the Fourier and pulse inputs are similar ($\rho = 0.117$ and 0.134, respectively; see Eq. (15)). Further, the time course of the decrease in order parameter is much faster for the Fourier than pulse input (Fig. 2, inset). In fact, the time durations required to reduce the order parameter below 0.4 are 213 and 514 ms for the Fourier and pulse inputs, respectively. These results suggest that stimulation with the Fourier input is more energy-efficient and disrupts synchronous activity faster than stimulation with the symmetric pulse input.

To more clearly compare the energy efficiency of the Fourier and symmetric pulse stimuli, the optimal solutions for the both stimuli were obtained with various values of the weight parameter α (Eq. (12)). Figure 3a, b show the values of the average order parameter ρ and the energy consumption rate E as functions of α for the cases of the Fourier (Fig. 3a) and symmetric pulse inputs (Fig. 3b). Note the difference in horizontal and vertical scales between these two panels. The results show that as α increases, the values of ρ and E tend to increase and decrease, respectively, for the both types of inputs, as expected from the objective function in Eq. (12). The relationship between ρ and E in Fig. 3c clarifies that the Fourier input requires less energy consumption than the symmetric pulse input when the same level of order parameter is attained. Additionally, we examined the optimization of an
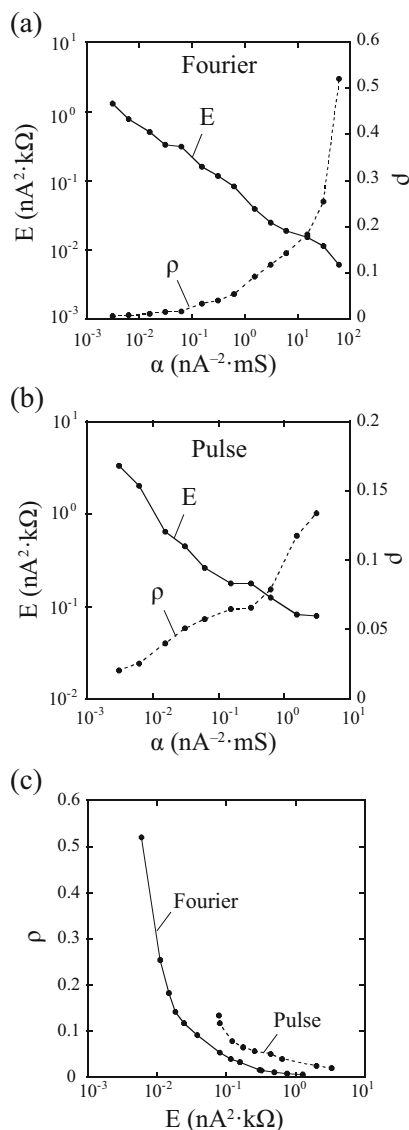
Fig. 3 The change in the average order parameter ρ and the energy consumption rate E obtained by optimization using various values of the weight parameter α. The value of α decides a relative balance between E and ρ in the objective function (Eq. (12)) such that larger and smaller values of α act to decrease the levels of E and ρ, respectively, through optimization. (a and b) The values of E (solid) and ρ (dashed) as function of α for the cases with Fourier (a) and symmetric pulse (b) inputs. (c) The relationship between ρ and E for the cases with Fourier (solid) and symmetric pulse (dashed) inputs. In (b), the E value converges to zero for $\alpha > 6$ nA^{-2}·mS, implying that the optimal pulse input is too small to be obtained by the current optimization method (see Methods). Therefore, the solution corresponding to this range of large α is omitted in (b) and in the dashed line in (c)

asymmetric pulse input that has more prolonged hyperpolarizing pulses (Eqs. 10 and 11; Fig. S1a) (Cogan 2008; Cogan et al. 2006; Fan et al. 2016; Hofmann et al. 2011). The results showed that the difference in the ρ and E values obtained with the symmetric and asymmetric pulses are not significant for many values of α (Fig. S1b), and thus the Fourier input is more energy efficient than both types of pulse inputs (Fig.

S1c). These results are in line with previous studies that suggest that the stimulating current with pulsatile waveforms may not be energy optimal for activating a neuron, as mentioned above (e.g., Forger et al. 2011; Grill 2015).

Additionally, Fig. 4 and Movies 1-3 (Supplementary Material) compare the firing pattern of the neuronal network without stimulation and with the optimal Fourier stimuli obtained using different values of the weight parameter α. The synchronous activity found in the absence of stimulus (Fig. 4a and Movie 1) is changed to relatively randomized activity by applying a moderate level of stimulus, which is obtained with relatively large α ($\alpha = 3.1$ nA^{-2}·mS) (Fig. 4b and Movie 2). In this case, the firing phases of neurons show higher variation, except for those near the corners of network at which the neural activity is highly affected by the input from the nearest electrode (Fig. 4b, right). The increase in the strength of stimulus induced by using a smaller value of α ($\alpha = 3.1 \times 10^{-3}$ nA^{-2}·mS) leads to a firing pattern that combines features of a traveling wave state and a clustered state (sometimes called a lurching wave; see Fig. 4c and Movie 3). In the presence of strong stimuli, the firing phases of all neurons are nearly fully governed by the input from the nearest electrode, as shown in Fig. 4c (right). Note that in the limit of $\alpha \to \infty$, the network state with the optimal stimulation matches the state without stimulus (Fig. 4a), because in this limit, the objective function in Eq. (12) is minimized by decreasing the E value to zero (without considering the ρ value) (Fig. 3a). Therefore, we can understand from Figs. 4a-c that the proposed method can generate firing patterns ranging from synchronous to randomized to lurching wave states as the α value is decreased from very large to small values. Figure 4d compares the waveforms of the optimized stimuli corresponding to four different values of α ($\alpha = 3.1$ (black), 3.1×10^{-1} (green), 3.1×10^{-2} (blue), and 3.1×10^{-3} nA^{-2}·mS (red)) on the same axis, where the peak current level is normalized to 1. The depolarizing phase of the current waveform is similar across the different values of α. On the other hand, the hyperpolarizing phase tends to fluctuate irregularly with changes in α, implying that the accuracy of optimization with the proposed method would not be high enough to discriminate a precise change in the optimal current waveform (but see also Discussion). The invariance of the waveform for the depolarizing phase likely arises because the time course of depolarization strongly affects the efficacy of neuronal activation (Foutz and McIntyre 2010) and therefore may be strictly regulated to achieve optimal order parameter reduction.

Previous studies (Tass 2003; Wilson and Moehlis 2014a) have examined the intermittent control of DBS, in which the stimulus is temporarily inactivated when the network is in a desynchronized state, and have shown that this technique is effective to improve the total energy efficiency. To examine the effectiveness of the intermittent control with the Fourier stimuli, we have obtained the relationship between ρ and E in

Fig. 4 Examples of the network firing pattern. (**a**) The case without current stimulation. (**b** and **c**) The cases with optimal Fourier inputs with moderate (**b**) and strong (**c**) intensity. The current waveform is obtained through optimization with the weight parameter $\alpha = 3.1$ (b) and 3.1×10^{-3} nA^{-2}·mS (c). In (a)-(c), the left and right figures show the raster plot and the distribution of the firing phase (ϕ_j in Eq. (14)), respectively. In the raster plot, the x-marks shown with the same color correspond to the neurons in the same quadrant in the x-y plane. The average order parameter for each panel is $\rho = 0.914$ (**a**), 0.117 (**b**), and 0.0061 (**c**). (**d**) The waveforms of the optimal Fourier current obtained with $\alpha = 3.1$ (black), 3.1×10^{-1} (green), 3.1×10^{-2} (blue) and 3.1×10^{-3} nA^{-2}·mS (red), where the peak value is normalized to 1. (The black and red lines correspond to the stimulus waveforms for (**b**) and (**c**), respectively.) The length of the double-headed arrow indicates the period T of the periodic current shown with the same color
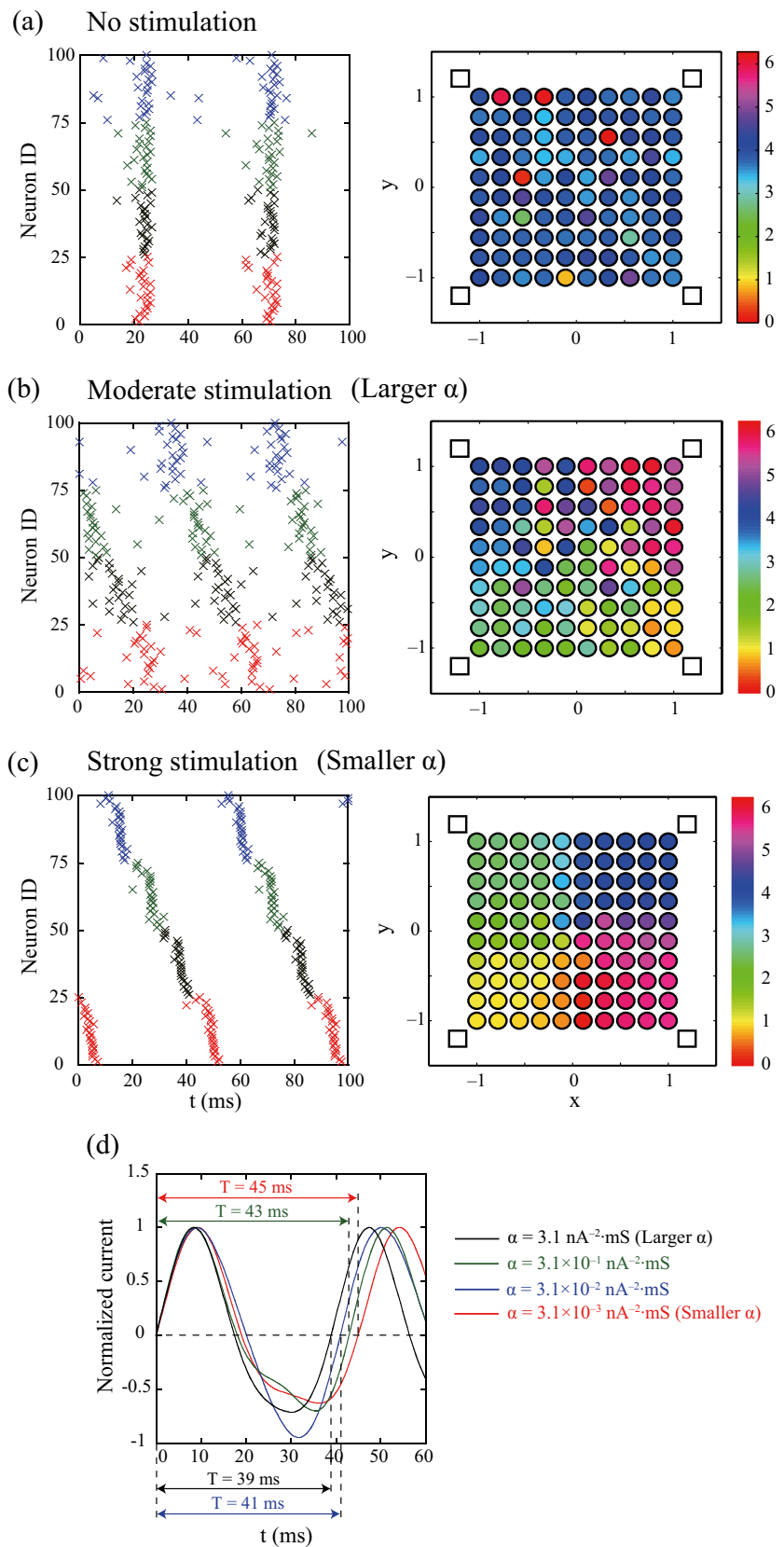
cases where the Fourier inputs, which are optimized with various α values, were periodically switched on and off. As shown in Fig. S2c, the level of energy consumption is always greater in the presence (red solid line) than the absence (black

solid line) of the intermittent control when the same level of order parameter is achieved. We found that the decrease in the energy efficiency of the Fourier stimuli due to the intermittent control is a robust outcome across various values of the time duration of the active and inactive phases. Further, the intermittent regulation was found to significantly degrade the energy efficiency of the optimal pulsatile inputs (Fig. S2c, dashed lines). These results would be attributable to the fact that the inactivation of stimulus for even a brief period causes a rapid increase in the order parameter, as in the examples of Figs. S2a and S2b. Considering that such rapid change to a synchronized state, in the absence of stimulation, is not found in the previous studies mentioned above (Tass 2003; Wilson and Moehlis 2014a), the effectiveness and efficiency of intermittent control methods could depend on the time course of synchronization, which would be intrinsic to the network dynamics in the absence of stimulating currents.

3.2 The effect of network properties on the efficacy of CR stimulation

The optimization procedure used proceeds by modulating the current waveform and directly evaluating a measure of the resultant change in the network dynamics. This direct optimization scheme has an advantage that almost arbitrary changes in the network dynamics can be handled by the optimization process (see also Discussion). By exploiting this feature, here we examine the effects of common oscillatory inputs, representing signals from other brain areas (Fig. 5), and of non-random connectivity (Fig. 6) on the efficacy of the CR modulation with the Fourier stimuli. The former step is motivated by the observation that pathological brain states such as parkinsonism are associated not only with increased synchronization but also with the emergence of abnormally strong oscillations, while the latter step is based on findings that neuronal synaptic connectivity patterns can deviate significantly from random.

In Fig. 5a (solid lines), we compared the relationship between ρ and E (as in Fig. 3c, solid line) for scenarios with and without common oscillatory inputs (see Methods). The amplitude of the common inputs oscillates with a frequency of 25 Hz, which is intended to resemble the beta-band (10–35 Hz) oscillation found in the basal ganglia-cortical loop in parkinsonism (Rubin et al. 2012; Mallet et al. 2008; Gatev et al. 2006). Our results (Fig. 5a, solid lines) show that the electrical energy required for attaining a given level of order parameter becomes larger in the presence of the common oscillatory activity; however, with enough energy, low levels of the order parameter can be induced even with common input present. In addition, as shown in Fig. 5b, the required energy level is significantly increased by increasing the intensity of the common stimuli. This result would be attributed to the fact that the common inputs tend to synchronize neurons through

harmonizing their firing phase (Türker and Powers 2001; Feng et al. 2000) and therefore can enhance the robustness of the synchronized state against stimulation. Additionally, as shown in Fig. 5c, the period of the optimal stimulating current (red line) is generally different from that of common inputs (black line). Therefore, in the presence of common oscillatory inputs, the stimulating current will have to overcome the influence of the rhythmic activity for acquiring the control over the network dynamics. In addition, in cases where the current stimulus optimized in the absence of common inputs is applied to the network in their presence (Fig. 5a, dashed line), the energy efficiency for desynchronization was only slightly degraded compared to the case where the stimulus is both optimized and applied in the presence of common inputs (Fig. 5a, red solid line). This finding suggests that the stimulus optimized without considering the oscillatory activity has a certain degree of robustness against changes in input features, which is encouraging for the utility of optimization methods for stimulus design in neural environments. As shown in Fig. 5d, the comparison of the optimal stimulus waveform obtained with and without the common oscillatory inputs showed that the addition of common inputs mainly affects the hyperpolarizing phase of the waveform while slightly modulating the length of the period, consistent with the types of changes seen with changes in α in Fig. 4d.

Furthermore, we explored how the topology of network connectivity can affect the effectiveness of CR stimulation. Recent studies have suggested that the stimulation of the motor cortex of parkinsonian animals as well as advanced PD patients can improve the motor symptoms through decreasing the synchronized oscillatory activities in the basal ganglia-cortical loop (Drouot et al. 2004; Gaynor et al. 2008; Lavano et al. 2017). The treatment with MCS appears to be potentially promising as an alternative to DBS to the basal ganglia, since MCS is considered as a minimally invasive neuromodulation procedure (Lavano et al. 2017). Since cortical circuits could be characterized by small-world connectivity (Haeusler and Maass 2007; Bettencourt et al. 2007; Yu et al. 2008; Gerhard et al. 2011), we examined the network topology-dependent change in the efficacy of current stimulation by comparing results of the proposed method across random and small-world networks (Fig. 6a, b, respectively).

Figure 6c, d compare the distribution of firing phases in the two networks, for the cases of applying the optimal stimuli with almost the same level of current energy ($E = \sim 5.8 \times 10^{-3}$ nA$^2 \cdot$kΩ). We found that the random network exhibits a relatively randomized phase distribution corresponding to $\rho = 0.102$ (Fig. 6c), whereas the small-world network exhibits a phase distribution that features more order yet corresponds to a lower ρ value of 0.043 (Fig. 6d). This finding suggests that synchronous activity in the small-world network has lower robustness against desynchronizing inputs than that in
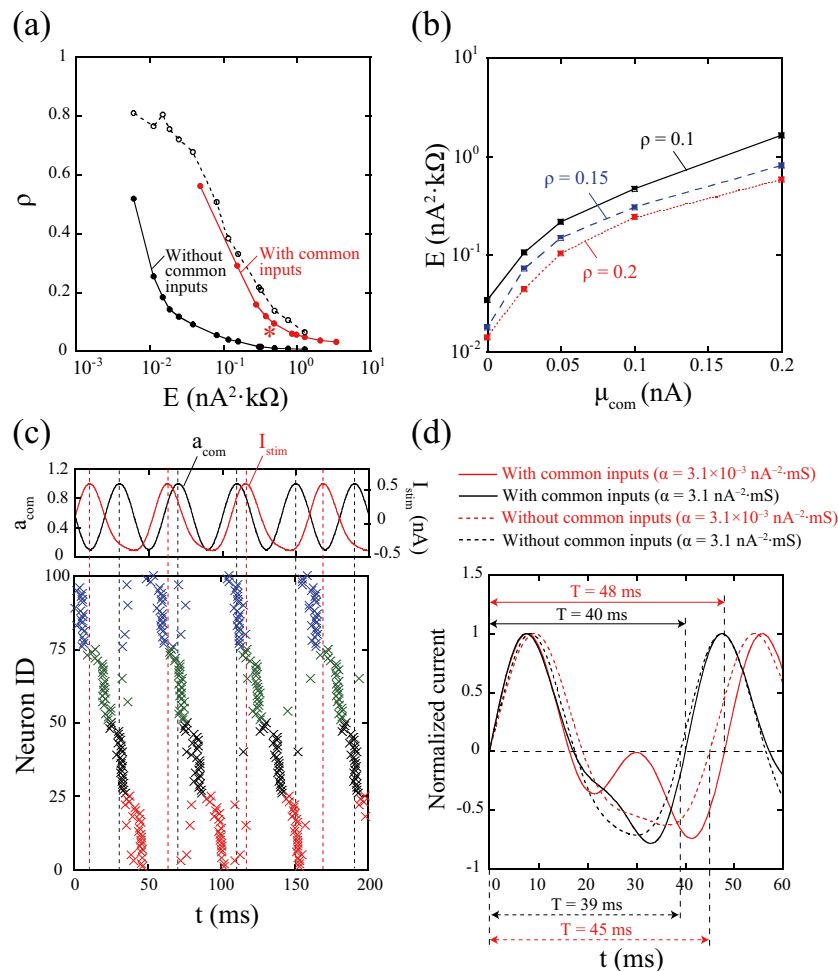
Fig. 5 The effect of common oscillatory inputs on the effectiveness of Fourier stimulation for desynchronization. (**a**) Solid lines: the relationship between the average order parameter ρ and the energy consumption rate E obtained by optimization with various values of α, for the cases of with (red) and without (black) common inputs. The strength parameter for the common inputs is $\mu_{com} = 0.1$ nA. The point denoted by an asterisk ($E = 0.49$ nA²·kΩ and $\rho = 0.095$) represents the solution corresponding to (**c**). Dashed line: the ρ vs. E relationship obtained for the case where the current stimuli, which are optimized with changing α values in the absence of common inputs, are applied in the presence of common inputs. (**b**) The levels of E required for achieving three different levels of ρ are plotted as functions of the mean of the shared white Gaussian noise distribution μ_{com} ($\rho = 0.1$ (black), 0.15 (blue), or 0.2 (red)). These curves are obtained by using the linear interpolation of the ρ vs. E relationship, obtained from optimization, for each μ_{com}. (**c**) The lower figure shows the

raster plot of the neurons receiving the optimal stimulus in the presence of common inputs ($\mu_{com} = 0.1$ nA and $\alpha = 0.16$ nA⁻²·mS). The x-marks with the same color correspond to the neurons in the same quadrant in the x-y plane. The upper figure shows the time course of the common inputs (a_{com} in Eq. (3); black) and one of the four stimulating currents (I_{stim}^{j} in Eq. 4; red). The vertical dashed lines represent the timings at which each current takes its peak value. (**d**) Examples of the optimized current waveform for $\alpha = 3.1$ (black) and 3.1×10^{-3} nA⁻²·mS (red), where the peak value is normalized to 1. The solid lines show the cases with the common inputs ($\mu_{com} = 0.1$ nA). The dashed lines show the cases without the common inputs (the same as shown in Fig. 4d with the same color). The length of the double-headed arrow represents the period T of the periodic current shown with the same color and line style

the random network. To more clearly show the comparison, Fig. 6e presents the relationship of ρ vs. E for the two types of networks and confirms that the electrical energy required for desynchronization is considerably smaller for the small-world (red line) than for the random network (black solid line). Here, we also plotted for several different values of α the characteristics of a modified random network in which the neural connection is randomly decided under the condition that the numbers of uni- and bidirectional connections between

neuron pairs are the same as those of the small-world network (see Methods). The result suggests that the ρ vs. E relationship for the modified random network (Fig. 6e, blue line) is nearly the same as that for the usual random network (Fig. 6e, black solid line). Thus, the lower robustness of the synchronized state against current stimulation in the small-world network is attributable not to the change in the numbers of uni- and bidirectional connections but to the change in the connection topology. Additionally, as shown in Fig. 6e

Fig. 6 The effect of network topology on the effectiveness of the Fourier stimuli for desynchronization. (**a** and **b**) The neural connections of the random (**a**) and small-world (**b**) networks. (**c** and **d**) The distribution of the firing phases of neurons (ϕ_j in Eq. (14)) when the optimized current is applied to the random (**c**) and small-world (**d**) networks. (**e**) Black and red solid lines: the relationship between the average order parameter ρ and the energy consumption rate E obtained by optimization with various values of α, for the cases with random (black) and small-world (red) connectivity. Blue dotted line: the ρ vs. E relationship obtained by optimization with changing α for the case with a connectivity that is randomly selected under the condition that the total numbers of uni- and bidirectional connections are the same as those in the small-world network. Black dashed line: the ρ vs. E relationship for the case where the inputs, which are optimized with the random network with changing α, are applied to the small-world network. (**f**) Examples of the optimized current waveform obtained with the random (dashed) and small-world (solid) networks, where the peak value is normalized to 1 ($\alpha=$ 3.1 (black) and 3.1×10^{-3} nA^{-2}·mS (red)). The length of the double-headed arrow indicates the period T of the periodic current shown with the same color and line style
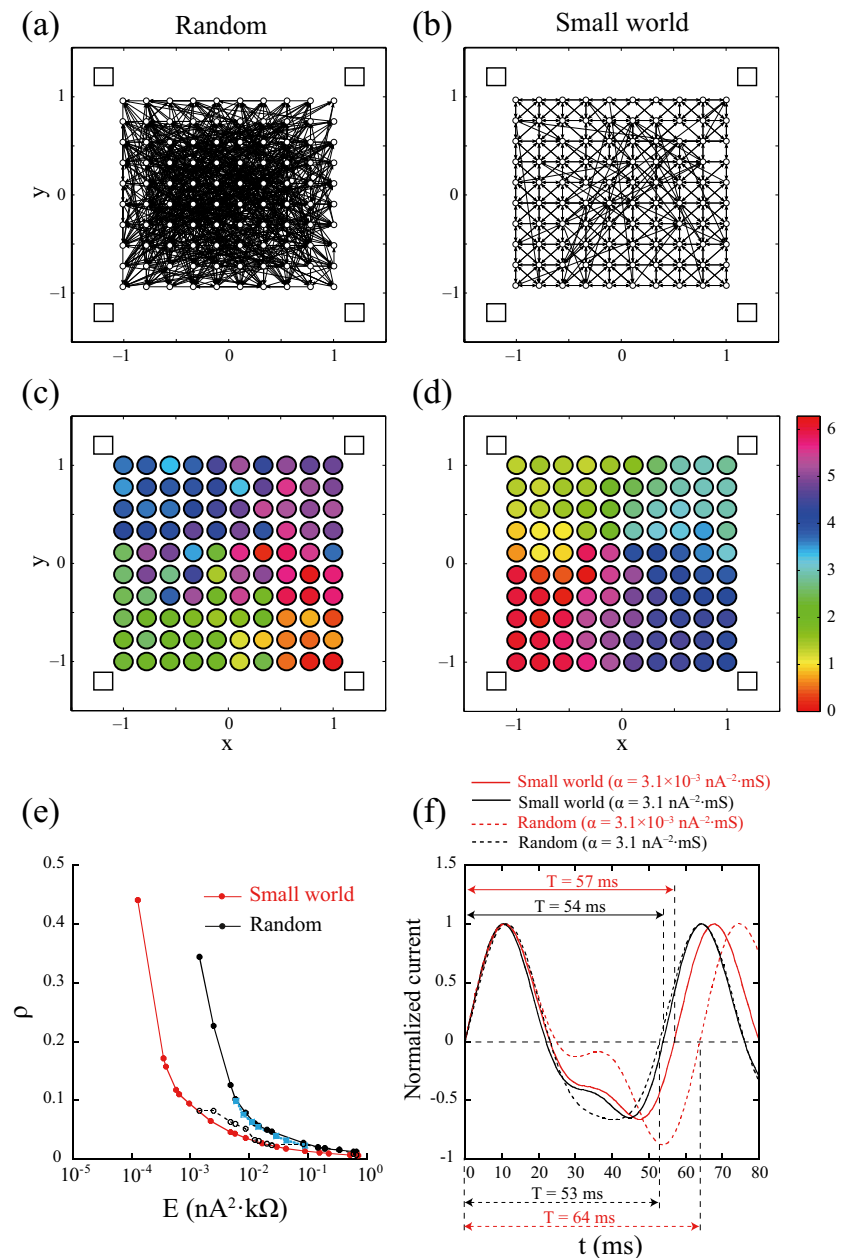
(black dashed line), when the stimulus optimized with the random network was applied to the small-world network, the ρ vs. E curve was found to lie between the two curves for which the stimulus was both optimized and applied in the identical networks (Fig. 6e, black and red solid lines). We also compared the optimized current waveform obtained using random and small-world networks. Figure 6f suggests that the change in network topology significantly affects the hyperpolarizing phase of the waveform almost without changing the depolarizing phase, as in the case when common oscillatory inputs were included (Fig. 5d). Overall, these results suggest that such non-random topology in neural circuits could modulate the optimal waveform of brain stimulation and its efficacy for

producing a desynchronized state, as well as the nature of the desynchronized state that emerges.

4 Discussion

Decreasing the current requirements of brain stimulating devices implanted for therapeutic interventions is an important goal that will prolong battery lives and reduce stimulation-induced side effects (Foutz and McIntyre 2010; Benabid et al. 2009). In this study, we addressed this issue using the approach of numerical optimization. In the proposed optimization method, the waveform of CR simulation is described as a second-order Fourier series with the constant term removed,

and the Fourier coefficients and the period are optimized to reduce the current energy required for achieving a desynchronized state, quantified by a standard order parameter. We demonstrate that after optimization, a Fourier input requires less energy consumption than does a conventional pulse input for attaining a given level of order parameter (Fig. 3c).

Our results show that the application of moderate and stronger intensity Fourier stimuli can change synchronized activity into relatively randomized and lurching wave activities, respectively (Fig. 4 and Movies 1-3). In the lurching wave pattern, the firing times of neurons are regulated almost deterministically by the electrode current activation. The emergence of this type of unnatural regular pattern would be a limitation of the proposed method, which is based on the use of an order parameter to measure synchrony, and also should be considered in interpreting other computational studies of stimulation involving this order parameter. In addition, it should be kept in mind that the relationship between the level of the order parameter and the symptoms of movement disorder has not yet been established. Although the proposed stimulation method is energy efficient for decreasing the order parameter, the interpretation of this result with respect to treatment of PD should be made with care. In the future work, it would be important to involve a measure that specifically quantifies the extent of the pathological activity pattern in parkinsonism. It is possible that features of basal ganglia activity other than synchrony, such as downstream impacts of basal ganglia inhibitory output (Rubin and Terman 2004) or alterations in oscillatory power (Kühn et al. 2008), may be more important than synchrony for inducing parkinsonian symptoms. It has been shown computationally that CR stimulation may significantly affect the former (Guo and Rubin 2011), and an immediate direction for future work could be to optimize CR stimulation with respect to cost functions designed based on this concept (cf. Feng et al. 2007).

We also applied the proposed optimization framework to examine how the effectiveness of current stimulation can be modulated by changes in network properties. We showed that when common oscillatory inputs are presented to the network, the desynchronizing stimulus becomes less effective, implying that the common inputs can strengthen the robustness of synchronous activity in the presence of applied current stimulation (Fig. 5). Standard DBS approaches ignore inputs to the targeted area, assuming that local and downstream effects of DBS will override pathological activity patterns occurring upstream. Our results offer a reminder that large-scale, system-wide effects of interventions may be important to consider, and extending our methods to models involving a more complete cortical-basal ganglia-thalamic loop (Dovzhenok and Rubchinsky 2012; Santaniello et al. 2015) would be a step in this direction, albeit with a potentially heavy computational cost for the optimization procedure.

Our results demonstrate that stimulation is more effective for desynchronization in a small-world than in a random network, suggesting that small-world connectivity can lead to the weakening of the robustness of synchrony (Fig. 6). This result is consistent with the general notion that randomly connected networks synchronize more easily than more structured networks, but it was not an obvious outcome in light of results showing that small-world oscillator networks generated from lattices via a small number of rewirings can in some conditions achieve similar or even improved synchronizability relative to random networks (Barahona and Pecora 2002; Hong et al. 2002). Our results suggest that the efficacy of brain stimulation used in the PD treatment could be highly affected by connectivity patterns at the stimulation site and thus highlight a possible pitfall of applying stereotyped stimulation patterns across a variety of brain areas. On the other hand, we found that for some energy levels, a similar reduction in order parameter resulted from using the optimal stimulus derived from both random and small-world networks to stimulate small-world networks (Fig. 6e). This result offers hope that even though full details of network connectivity are not experimentally accessible, optimization based on approximate connectivity patterns could still yield useful results and thus supports the practical utility of our methods. In the future, our approach could be used to study various other factors that can modulate network synchronization properties or responses to stimulation, such as the microstructural pattern in the frontal cortex (Muthuraman et al. 2017).

In this paper, we optimized stimulation waveforms for a neuronal network with recurrent excitatory synaptic connections between neurons. The inclusion of local excitatory synapses is relevant for thalamic networks, which are sites of stimulation for tremor (Ondo et al. 1998; Kumar et al. 2003; Baizabal-Carvallo et al. 2014), and cortical networks, which are under investigation as targets for stimulation for parkinsonian conditions (Drouot et al. 2004; Gaynor et al. 2008; Rosin et al. 2011; Lavano et al. 2017). It would be interesting, and relevant for STN-DBS under parkinsonian conditions, to consider a network lacking excitatory connections and exhibiting synchrony due only to common inputs or a network including an inhibitory population, to represent the STN-globus pallidus loop (Terman et al. 2002).

The problem of searching for energy-optimal current waveforms has been receiving interest, due to its importance in finding suitable stimulus delivery methods for implantable neural stimulators (Jezernik and Morari 2005; Sahin and Tie 2007; Jezernik et al. 2010; Foutz and McIntyre 2010; Wongsarnpigoon et al. 2010; Wongsarnpigoon and Grill 2010; Forger et al. 2011; see Grill 2015 for review). Recent studies by Wilson and Moehlis (2014a, b) have applied optimal control theory to find energy-optimal stimuli that endow neuronal membrane dynamics with a positive Lyapunov exponent and thereby produce desynchronization. The approach

of controlling the Lyapunov exponent is useful to substantially desynchronize network activity by using just a single DBS electrode with less energy consumption. But, optimal control theory generally involves the solution of the Euler-Lagrange equation, which is derived by differentiation of a modified objective function including constraints (Dixon 1972). Since the neuronal dynamics needs to be simply described in the modified objective function, it would be difficult to fully consider complicated network dynamics in this optimization process. In contrast, in our proposed optimization method, the class of stimulation patterns is directly explored by modulating the current waveform and estimating the resultant change in the order parameter from numerical simulation. This approach allows the consideration of CR stimulation involving multiple stimulation sites and of various changes in the network dynamics, as demonstrated by the simulations in Figs. 5 and 6.

A disadvantage of our optimization method is that it takes long time to search for a solution which can be adequately considered to be globally optimal (see Methods for computation time). Moreover, it is generally difficult to ensure the global optimality of solutions. As mentioned above, the optimized current waveform was shown to change irregularly with changing the weight parameter in our objective function (Fig. 4d), which would imply the involvement of locally (but not globally) optimal solutions. We note, however, that the order parameter and energy associated with our optimal waveform depended relatively smoothly on the weight parameter (Fig. 3) and varied smoothly with parameter changes as we explored common inputs and network topologies (Figs. 5 and 6), despite the fact that for each simulation, we repeated the pattern search 8 times from independent, randomly selected starting points. This smooth dependence provides some reassurance that our results are not dominated by convergence to locally optimal solutions far from global optima, since it is highly unlikely that such local optima, attained from independent starting point, would yield such regular changes in order parameter and stimulation energy. Interestingly, the variability that we did observe across optimal stimulus waveforms was always associated with the hyperpolarizing phase, suggesting that focusing on this phase might make sense for the design of waveforms in future settings.

It is important to note several limitations of this study. A main limitation of the proposed optimization scheme is that the stimulus waveform is composed of low-order Fourier coefficients (with the maximum degree $p = 2$ in Eq. 5), meaning that the precise waveforms of optimal stimuli, represented by higher order coefficients, cannot be obtained. Although the charge balance is maintained in the proposed Fourier input to avoid electrode and tissue damage, charge balancing is a necessary but not sufficient condition for safe stimulation (Cogan 2008; Cogan et al. 2006). Large potential excursions during the delivery of stimulating currents can induce irreversible reduction and oxidation reactions that are harmful to the electrode

and tissue. Therefore, adequately setting higher-order Fourier coefficients could be important not only for allowing exploration of a broader range of stimulation waveforms but also for regulating the current injection on shorter time scales to prevent these side effects.

Another limitation is that the current study is based on a network model composed of simplified LIF neurons, which allows for proof of the principle of the optimization approach but may not be sufficient for providing quantitative predictions. Some previous works illustrate the importance of nonlinear properties of membrane conductances for determining the optimal current waveform for activating neurons (Forger et al. 2011; Wongsarnpigoon et al. 2010). In addition to considering neuronal nonlinearities, practical application of this work would require extension to represent extracellular current-controlled stimulation conditions (Foutz and McIntyre 2010). A detailed computational model by Foutz and McIntyre (2010) studied the effectiveness of stimulating currents with various waveforms for activating neurons. Their results suggest that relative effectiveness of different current waveforms does not fundamentally depend on whether an intracellular or extracellular stimulation condition is used. However, they also show that the temporal width of the optimal current stimulus could change depending on the stimulation conditions. Therefore, to improve the accuracy of the time course of the optimal CR stimulation, it may be necessary to include the mechanisms of current flow passing through the neural membrane and the extracellular media surrounding the neurons as in *in vivo* situations. Simulating the current stimulation under more natural *in vivo* conditions also serves to provide the basis for designing actual implantable systems, which need to satisfy various tight constraints, such as those on energy consumption considered in this study as well as others on the device size and processing capacity (Greenwald et al. 2016; Wise et al. 2008).

Compliance with ethical standards

Conflict of interest The authors declare that they have no conflict of interest.

References

Adamchic, I., Hauptmann, C., Barnikol, U. B., Pawelczyk, N., Popovych, O., Barnikol, T. T., Silchenko, A., Volkmann, J., Deuschl, G., Meissner, W. G., Maarouf, M., Sturm, V., Freund, H. J., & Tass, P. A. (2014). Coordinated reset neuromodulation for Parkinson's disease: Proof-of-concept study. *Movement Disorders, 29*, 1679–1684.

Baizabal-Carvallo, J. F., Kagnoff, M. N., Jimenez-Shahed, J., Fekete, R., & Jankovic, J. (2014). The safety and efficacy of thalamic deep brain

stimulation in essential tremor: 10 years and beyond. *Journal of Neurology Neurosurgery and Psychiatry, 85*, 567–572.

Barahona, M., & Pecora, L. M. (2002). Synchronization in small-world systems. *Physical Review Letters, 89*, 054101.

Benabid, A. L., Chabardes, S., Mitrofanis, J., & Pallak, P. (2009). Deep brain stimulation of the subthalamic nucleus for the treatment of Parkinson's disease. *The Lancet Neurology, 8*, 67–81.

Bettencourt, L. M. A., Stephens, G. J., Ham, M. I., & Gross, G. W. (2007). Functional structure of cortical neuronal networks grown *in vitro*. *Physical Review E, 75*, 021915.

Brocker, D. T., Swan, B. D., So, R. Q., Turner, D. A., Gross, R. E., & Grill, W. M. (2017). Optimized temporal pattern of brain stimulation designed by computational evolution. *Science Translational Medicine, 9*, eaah3532.

Cogan, S. F. (2008). Neural stimulation and recording electrodes. *Annual Reviews of Biomedical Engineering, 10*, 275–309.

Cogan, S. F., Troyk, P. R., Ehrlich, J., Plante, T. D., & Detlefsen, D. E. (2006). Potential-biased, asymmetric waveforms for charge-injection with activated iridium oxide (AIROF) neural stimulation electrodes. *IEEE Transactions on Biomedical Engineering, 53*, 327–332.

Dixon, L. C. W. (1972). *Nonlinear optimization*. London: The English Universities Press.

Dovzhenok, A., & Rubchinsky, L. L. (2012). On the origin of tremor in Parkinson's disease. *PLoS One, 7*, e41598.

Drouot, X., Oschino, S., Jarraya, B., Besret, L., Kishima, H., Remy, P., Dauguet, J., Lefaucheur, J. P., Dolle, F., Conde, F., Bottlaender, M., Peschanski, M., Keravel, Y., Hantraye, P., & Palfi, S. (2004). Functional recovery in a primate model of Parkinson's disease following motor cortex stimulation. *Neuron, 44*, 769–778.

Ebert, M., Hauptmann, C., & Tass, P. A. (2014). Coordinated reset stimulation in a large-scale model of the STN-GPe circuit. *Frontiers in Computational Neuroscience, 8*, 154.

Fan, D., Wang, Z., & Wang, Q. (2016). Optimal control of directional deep brain stimulation in the parkinsonian neuronal network. *Communications in Nonlinear Science and Numerical Simulation, 36*, 219–237.

Feng, J., Brown, D., & Li, G. (2000). Synchronization due to common pulsed input in Stein's model. *Physical Review E, 61*, 2987–2995.

Feng, X. J., Greenwald, B., Rabitz, H., Shea-Brown, E., & Kosut, R. (2007). Toward closed-loop optimization of deep brain stimulation for Parkinson's disease: concepts and lessons from a computational model. *Journal of Neural Engineering, 4*(2), L14–L21.

Forger, D. B., Paydarfar, D., & Clay, J. R. (2011). Optimal stimulus shapes for neuronal excitation. *PLoS Computational Biology, 7*, e1002089.

Foutz, T. J., & McIntyre, C. C. (2010). Evaluation of novel stimulus waveforms for deep brain stimulation. *Journal of Neural Engineering, 7*, 066008.

Gatev, P., Darbin, O., & Wichmann, T. (2006). Oscillations in the basal ganglia under normal conditions and in movement disorders. *Movement Disorders, 21*, 1566–1677.

Gaynor, L. M. F. D., Kühn, A. A., Dileone, M., Litvak, V., Eusebio, A., Pogosyan, A., Androulidakis, A. G., Tisch, S., Limousin, P., & Insola, A. (2008). Suppression of beta oscillations in the subthalamic nucleus following cortical stimulation in humans. *European Journal of Neuroscience, 28*, 1686–1695.

Gerhard, F., Pipa, G., Lima, B., Neuenschwander, S., & Gerstner, W. (2011). Extraction of network topology from multi-electrode recordings: is there a small-world effect? *Frontiers in Computational Neuroscience, 5*, 4.

Greenwald, E., Masters, M. R., & Thakor, N. V. (2016). Implantable neurotechnologies: bidirectional neural interfaces–applications and VLSI circuit implementations. *Medical and Biological Engineering and Computing, 54*, 1–17.

Grill, W. M. (2015). Model-based analysis and design of waveforms for efficient neural stimulation. *Progress in Brain Research, 222*, 147–162.

Guo, Y., & Rubin, J. E. (2011). Multi-site stimulation of subthalamic nucleus diminishes thalamocortical relay errors in a biophysical network model. *Neural Networks, 24*(6), 602–616.

Haeusler, S., & Maass, W. (2007). A statistical analysis of information-processing properties of lamina-specific cortical microcircuit models. *Cerebral Cortex, 17*, 149–162.

Herrington, T. M., Cheng, J. J., & Eskandar, E. N. (2016). Mechanisms of deep brain stimulation. *Journal of Neurophysiology, 115*, 19–38.

Hofmann, L., Ebert, M., Tass, P. A., & Hauptmann, C. (2011). Modified pulse shapes for effective neural stimulation. *Frontiers in Neuroengineering, 4*, 9.

Hong, H., Choi, M. Y., & Kim, B. J. (2002). Synchronization on small-world networks. *Physical Review E, 65*, 026139.

Hooke, R., & Jeeves, T. A. (1961). Direct search solution of numerical and statistical problems. *Journal of Association of Computing Machinery, 8*, 212–229.

Izhikevich, E. M., Gally, J. A., & Edelman, G. M. (2004). Spike-timing dynamics of neuronal groups. *Cerebral Cortex, 14*, 933–944.

Jezernik, S., & Morari, M. (2005). Energy-optimal electrical excitation of nerve fibers. *IEEE Transactions on Biomedical Engineering, 52*, 740–743.

Jezernik, S., Sinkjaer, T., & Morari, M. (2010). Charge and energy minimization in electrical/magnetic stimulation of nervous tissue. *Journal of Neural Engineering, 7*, 046004.

Khambampati, A. K., Ijaz, U. Z., Lee, J. S., Kim, S., & Kim, K. Y. (2010). Phase boundary estimation in electrical impedance tomography using the Hooke and Jeeves pattern search method. *Measurement Science and Technology, 21*, 035501.

Kubota, S., Kanomata, K., Suzuki, T., Ahmmad, B., & Hirose, F. (2015). Hybrid antireflection structure with moth eye and multilayer coating for organic photovoltaics. *Journal of Coatings Technology and Research, 12*, 37–47.

Kühn, A. A., & Volkmann, J. (2017). Innovations in deep brain stimulation methodology. *Movement Disorders, 32*, 11–19.

Kühn, A. A., Kempf, F., Brücke, C., Doyle, L. G., Martinez-Torres, I., Pogosyan, A., Trottenberg, T., Kupsch, A., Schneider, G. H., Hariz, M. I., Vandenberghe, W., Nuttin, B., & Brown, P. (2008). High-frequency stimulation of the subthalamic nucleus suppresses oscillatory β activity in patients with Parkinson's disease in parallel with improvement in motor performance. *Journal of Neuroscience, 28*(24), 6165–6173.

Kumar, R., Lozano, A. M., Sime, E., & Lang, A. E. (2003). Long-term follow-up of thalamic deep brain stimulation for essential and parkinsonian tremor. *Neurology, 61*, 1601–1604.

Kuncel, A. M., & Grill, W. M. (2004). Selection of stimulus parameters for deep brain stimulation. *Clinical Neurophysiology, 115*, 2431–2441.

Lavano, A., Guzzi, G., De Rose, M., Romano, M., Della Torre, A., Vescio, G., Deodato, F., Lavano, F., & Volpentesta, G. (2017). Minimally invasive motor cortex stimulation for Parkinson's disease. *Journal of Neurosurgical Sciences, 61*, 77–87.

Liu, Y. H., & Wang, X. J. (2001). Spike-frequency adaptation of a generalized leaky integrate-and-fire model neuron. *Journal of Computational Neuroscience, 10*, 25–45.

Mallet, N., Pogosyan, A., Sharott, A., Csicsvari, J., Bolam, J. P., Brown, P., & Magill, P. J. (2008). Disrupted dopamine transmission and the emergence of exaggerated beta oscillations in subthalamic nucleus and cerebral cortex. *Journal of Neuroscience, 28*, 4795–4806.

Muthuraman, M., Deuschl, G., Koirala, N., Riedel, C., Volkmann, J., & Groppa, S. (2017). Effects of DBS in parkinsonian patients depend on the structural integrity of frontal cortex. *Scientific Reports, 7*, 43571.

Ondo, W., Jankovic, J., Schwartz, K., Almaguer, M., & Simpson, R. K. (1998). Unilateral thalamic deep brain stimulation for refractory

essential tremor and Parkinson's disease tremor. *Neurology, 51*, 1063–1069.

Prettejohn, B. J., Berryman, M. J., & McDonnell, M. D. (2011). Methods for generating complex networks with selected structural properties for simulations: A review and tutorial for neuroscientists. *Frontiers in Computational Neuroscience, 5*, 11.

Reich, M. M., Steigerwald, F., Sawalhe, A. D., Reese, R., Gunalan, K., Johannes, S., Nickl, R., Matthies, C., McIntyre, C. C., & Volkmann, J. (2015). Short pulse width widens the therapeutic window of subthalamic neurostimulation. *Annals of Clinical and Tranlational Neurology, 2*, 427–432.

Rosin, B., Slovik, M., Mitelman, R., Rivlin-Etzion, M., Haber, S. N., Israel, Z., Vaadia, E., & Bergman, H. (2011). Closed-loop deep brain stimulation is superior in ameliorating parkinsonism. *Neuron, 72*, 370–384.

Rubin, J. E., & Terman, D. (2004). High frequency stimulation of the subthalamic nucleus eliminates pathological thalamic rhythmicity in a computational model. *Journal of Computational Neuroscience, 16*(3), 211–235.

Rubin, J. E., McIntyre, C. C., Turner, R. S., & Wichmann, T. (2012). Basal ganglia activity patterns in parkinsonism and computational modeling of their downstream effects. *European Journal of Neuroscience, 36*, 2213–2228.

Sahin, M., & Tie, Y. (2007). Non-rectangular waveforms for neural stimulation with practical electrodes. *Journal of Neural Engineering, 4*, 227–233.

Santaniello, S., McCarthy, M. M., Montgomery, E. B., Gale, J. T., Kopell, N., & Sarma, S. V. (2015). Therapeutic mechanisms of high-frequency stimulation in Parkinson's disease and neural restoration via loop-based reinforcement. *Proceedings of the National Academy of Sciences of the United States of America, 112*, E586–E595.

Tass, P. A. (2003). A model of desynchronizing deep brain stimulation with a demand-controlled coordinated reset of neural subpopulations. *Biological Cybernetics, 89*, 81–88.

Tass, P. A., Qin, L., Hauptmann, C., Dovero, S., Bezard, E., Boraud, T., & Meissner, W. G. (2012). Coordinated reset has sustained aftereffects in Parkinsonian monkeys. *Annals of Neurology, 72*, 816–820.

Terman, D., Rubin, J. E., Yew, A. C., & Wilson, C. J. (2002). Activity patterns in a model for the subthalamopallidal network of the basal ganglia. *Journal of Neuroscience, 22*, 2963–2976.

Troyer, T. W., & Miller, K. D. (1997). Physiological gain leads to high ISI variability in a simple model of a cortical regular spiking cell. *Neural Computation, 9*, 971–983.

Türker, K. S., & Powers, R. K. (2001). Effects of common excitatory and inhibitory inputs on motoneuron synchronization. *Journal of Neurophysiology, 86*, 2807–2822.

Wang, J., Nebeck, S., Muralidharan, A., Johnson, M. D., Vitek, J. L., & Baker, K. B. (2016). Coordinated reset deep brain stimulation of subthalamic nucleus produces long-lasting, dose-dependent motor improvements in the 1-methyl-4-phenyl-1,2,3,6-tetrahydropyridine non-human primate model of parkinsonism. *Brain Stimulation, 9*, 609–617.

Watts, D. J., & Strogatz, S. H. (1998). Collective dynamics of 'small-world' networks. *Nature, 393*, 440–442.

Wilson, D., & Moehlis, J. (2014a). Locally optimal extracellular stimulation for chaotic desynchronization of neural populations. *Journal of Computational Neuroscience, 37*, 243–257.

Wilson, D., & Moehlis, J. (2014b). Optimal chaotic desynchronization for neural populations. *SIAM Journal on Applied Dynamical Systems, 13*, 276–305.

Wise, K. D., Sodagar, A. M., Yao, Y., Gulari, M. N., Perlin, G. E., & Najafi, K. (2008). Microelectrodes, microelectronics, and implantable neural microsystems. *Proceedings of the IEEE, 96*, 1184–1202.

Wongsarnpigoon, A., & Grill, W. M. (2010). Energy-efficient waveform shapes for neural stimulation revealed with genetic algorithm. *Journal of Neural Engineering, 7*, 046009.

Wongsarnpigoon, A., Woock, J. P., & Grill, W. M. (2010). Efficiency analysis of waveform shape for electrical excitation of nerve fibers. *IEEE Transactions on Neural Systems and Rehabilitation Engineering, 18*, 319–328.

Yu, S., Huang, D., Singer, W., & Nikolic, D. (2008). A small world of neuronal synchrony. *Cerebral Cortex, 18*, 2891–2901.